

Signatures of a Conical Intersection in Attosecond Transient Absorption Spectroscopy

Jens E. Bækhøj,¹ Camille Lévêque,² and Lars Bojer Madsen²

¹*Department of Physics and Astronomy, Louisiana State University, Baton Rouge, Louisiana 70803, USA*

²*Department of Physics and Astronomy, Aarhus University, 8000 Aarhus C, Denmark*



(Received 11 April 2018; revised manuscript received 11 June 2018; published 11 July 2018)

We characterize attosecond transient absorption spectroscopy (ATAS) in molecules with coupled nuclear and electronic dynamics in the vicinity of a conical intersection between adiabatic potential energy surfaces. With respect to ATAS, the nonadiabatic vibronic coupling strength can be divided into weak, intermediate, and strong, and the characteristics of spectra belonging to each of these domains are discussed. The results can guide the analysis of ATAS experiments in molecules with conical intersections.

DOI: 10.1103/PhysRevLett.121.023203

In the Born-Oppenheimer approximation (BOA), electronic and nuclear degrees of freedom are separated and this separation offers a picture where the nuclei move on an adiabatic potential energy surface (PES) formed by the faster electrons. A conical intersection (CI) is a point in the configuration space of the nuclei in polyatomic molecules where two adiabatic PESs are degenerate. The local topology of the PESs at the CI is that of a double cone [1,2]. In the vicinity of the CI, the nonadiabatic coupling between the vibrational and electronic motion, i.e., the vibronic coupling (VC), becomes large, and the BOA breaks down. It is by now understood that CIs are abundant in polyatomic molecules and key in photophysical and photochemical molecular processes [3], e.g., in the ultrafast primary photoisomerization event in the vision [4]. Recently, coherent electron-hole wave packet dynamics were studied in CO₂ near a CI [5], two-dimensional electronic-vibrational spectroscopy was illustrated [6], and the nonadiabatic electron-nuclear dynamics was elucidated by theory on attosecond streaking [7] and attosecond stimulated x-ray Raman processes [8]. Very recently, the effects of nonadiabatic couplings on electronic coherences close to a CI were investigated [9].

As we shall see, attosecond transient absorption spectroscopy (ATAS) seems ideal for an investigation of CIs. In transient absorption spectroscopy, the frequency-resolved, time-integrated absorption by a medium interacting with two time-delayed laser pulses is measured. One pulse induces transient dynamics, which is imprinted onto the spectrum by the other pulse. Control of the relative delay between the two pulses gives the time resolution, while the width of the features being probed gives the spectral resolution. Because time is accessed indirectly via the measurement of a delay-dependent signal, transient absorption spectroscopy gives access to both fast dynamics and narrow spectra features without violating Fourier transform limits [10]. In ATAS, an attosecond pulse is displaced in time with respect to a femtosecond laser pulse, and they can

be synchronized with subfemtosecond resolution [10]. We use the notation near infrared (NIR) and extreme ultraviolet (XUV) to denote the femto- and attosecond pulses, respectively, although their wavelengths could be in different regimes. ATAS has proven to be excellent for the study of ultrafast subfemtosecond dynamics, not only in atoms [11–15], but also in molecules [16–20] and solids [21,22]. The signatures of nonadiabatic couplings between electronic and nuclear degrees of freedom have not been investigated by ATAS. It is the purpose of this Letter to highlight how the ultrafast nonadiabatic dynamics in the vicinity of a CI is revealed by specific signatures in ATAS.

To capture and highlight the rich dynamics near a CI, we consider a simple model Hamiltonian that describes a CI and still shares essential features with real molecules. The nuclear degrees of freedom are restricted to two dimensionless mass-frequency-scaled vibrational modes Q_1 and Q_2 [3]. We present ATAS spectra based on this model, which allows extensive parameter scans, and adjust the influence of the CI on the dynamics by varying the VC strength. We categorize the VC strength into weak, intermediate, and strong based on characteristic ATAS features for each of these domains. In the adiabatic representation, the nonadiabatic couplings appear through the action of the nuclear kinetic energy operator on the electronic wave functions and the couplings diverge at the CI. To avoid this divergence, the Hamiltonian is expressed in a diabatic representation where different electronic states $|\phi_j^{(d)}\rangle$ are coupled by smoothly varying off-diagonal elements of the potential matrix. In the vicinity of the CI, the two diabatic electronic surfaces involved in the CI are approximated as harmonic [23,24]. This two-surface diabatic VC model was introduced more than 40 years ago [23] and has been successfully applied ever since (see, e.g., Ref. [3]). Finally, for ATAS, we supplement the VC model with two additional diabatic surfaces, such that, in total, four surfaces are involved (Fig. 1). The Hamiltonian is represented as

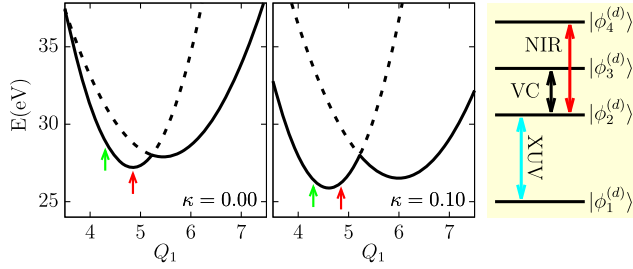


FIG. 1. Adiabatic PESs (see text) corresponding to the adiabatic $|\phi_2^{(a)}\rangle$ (full line) and $|\phi_3^{(a)}\rangle$ (dashed line) states for $\kappa = 0.0$ (left) and $\kappa = 0.1$ (middle) [see Eq. (3)] as a function of Q_1 for $\check{Q}_1 = 5.217$ and $Q_2 = \check{Q}_2 = 0$, which makes the figure independent of the interstate coupling γ . The green (red) arrow indicates the position of the minimum of the PES corresponding to the adiabatic $|\phi_1^{(a)}\rangle$ ($|\phi_4^{(a)}\rangle$) state. (Right) Illustrates the diabatic electronic states $|\phi_j^{(d)}\rangle$ and their couplings [see Eqs. (2) and (3)].

$$H_{ij} = \left(-\frac{\omega_{i,1}}{2} \frac{\partial^2}{\partial Q_1^2} - \frac{\omega_{i,2}}{2} \frac{\partial^2}{\partial Q_2^2} + V_i(Q_1, Q_2) \right) \delta_{ij} + V_{ij}^L(t) + \Delta V_{ij}(Q_1, Q_2), \quad (1)$$

with the PES for the i th diabatic state given by $V_i(Q_1, Q_2) = (\omega_{i,1}/2)(Q_1 - \check{Q}_{i,1})^2 + (\omega_{i,2}/2)(Q_2 - \check{Q}_{i,2})^2 + b_i$, with $\omega_{i,1}$ and $\omega_{i,2}$ as the frequencies, minimum at $(\check{Q}_{i,1}, \check{Q}_{i,2})$, along Q_1 and Q_2 , respectively, and b_i as the energy offset with respect to the ground state. Note that, while the diabatic surfaces are harmonic, the adiabatic are not (Fig. 1) and, as we shall see below, the spectra show clear anharmonic features. The parameters of the model are detailed in the Supplemental Material [25]. The laser interactions $V_{ij}^L(t)$ of Eq. (1) are

$$V^L(t) = \begin{bmatrix} 0 & d_{12}^{\text{el}} F_{\text{XUV}}(t) & 0 & 0 \\ d_{21}^{\text{el}} F_{\text{XUV}}(t) & 0 & d_{24}^{\text{el}} F_{\text{NIR}}(t) & 0 \\ 0 & 0 & 0 & 0 \\ 0 & d_{42}^{\text{el}} F_{\text{NIR}}(t) & 0 & 0 \end{bmatrix}, \quad (2)$$

where d_{ij}^{el} is the dipole transition moment between the i th and j th diabatic electronic states. For both $F_{\text{XUV}}(t)$ and $F_{\text{NIR}}(t)$, we use the expression $F(t) = F_0 \cos[\pi(t + \tau)/N_c T] \times \sin[\omega(t + \tau)]$, for $-N_c T/2 \leq t + \tau \leq N_c T/2$ with N_c as the number of cycles and T as the period. For the NIR pulse, $\tau = 0$ since its maximum is used as the time reference. With this definition of delay, a positive (negative) delay describes the situation when the XUV comes before (after) the NIR. The XUV and NIR are 50 and 800 nm fields with intensities of 10^9 and 5×10^{12} W/cm² and FWHM field strength durations of 330 as and 5.30 fs, respectively.

The nondiagonal elements $\Delta V_{ij}(Q_1, Q_2)$ in Eq. (1) contain the VCs. Here, $|\phi_2^{(d)}\rangle$ and $|\phi_3^{(d)}\rangle$ couple through ΔV_{23} (Fig. 1). We follow [24] and use

$$\Delta V(Q_1, Q_2) = \begin{bmatrix} 0 & 0 & 0 & 0 \\ 0 & \kappa(Q_1 - \check{Q}_1) & \gamma(Q_2 - \check{Q}_2) & 0 \\ 0 & \gamma(Q_2 - \check{Q}_2) & -\kappa(Q_1 - \check{Q}_1) & 0 \\ 0 & 0 & 0 & 0 \end{bmatrix}, \quad (3)$$

where \check{Q}_1 and \check{Q}_2 define the position of the CI. In Eq. (3), γ is the first-order interstate coupling constant, and it influences the VC strength and deforms the PESs in the Q_2 direction. The first-order intrastate coupling κ deforms the PESs in the Q_1 direction. The two left panels of Fig. 1 show the PESs in the Q_1 direction for two values of κ , and the right panel specifies the VC [Eq. (3)] and light-induced couplings [Eq. (2)]. The transformation from the diabatic $|\phi_j^{(d)}\rangle$ to the adiabatic $|\phi_j^{(a)}\rangle$ representation is done by diagonalizing the 4×4 potential matrix at each nuclear configuration, $V^{(a)} = UV^{(d)}U^\dagger$.

The VC model approximates the diabatic electronic surfaces with a low-order Taylor expansion in terms of normal coordinates. Usually, the coupling constants entering the Hamiltonian are evaluated using *ab initio* calculations for specific electronic states of a given molecule. Here, we do not attempt to describe a specific molecule, but aim at providing general features of ATAS spectra in the presence of a CI; thus, we perform a scan of these parameters. Because of the quadratic approximation of the diabatic surfaces, the model is not suitable for describing large amplitude nuclear motion, as, e.g., photoinduced dissociation processes. For dynamics where the nuclear wave packet explores a limited part of the PESs, as in the vicinity of the CI, the diabatic PESs are well approximated by low-order Taylor expansions and the model provides accurate results and has been successfully applied to understand spectra of many molecules with CIs [3].

For a given time delay τ , between the XUV and the NIR pulse, the absorption spectra are modeled by [28] $S(\omega, \tau) = (4\pi n \omega / c) \text{Im}[F_{\text{XUV}}^*(\omega, \tau) d(\omega, \tau)]$, with n as the density of molecules, c as the speed of light, and $F_{\text{XUV}}(\omega, \tau)$ and $d(\omega, \tau)$ as the Fourier transforms of the XUV pulse and the expectation value of the dipole operator $d(t, \tau)$, respectively [29]. To obtain $d(t, \tau)$, we propagate the time-dependent Schrödinger equation with the Hamiltonian of Eq. (1) by a fast Fourier transform split-operator algorithm [25,30]. Since $|\phi_2^{(d)}\rangle$ is the only excited state with a nonzero dipole coupling to the ground state (Fig. 1), $d(t, \tau)$ and thereby the absorption spectrum is a direct measure of the phase and population of the $|\phi_2^{(d)}\rangle$ state.

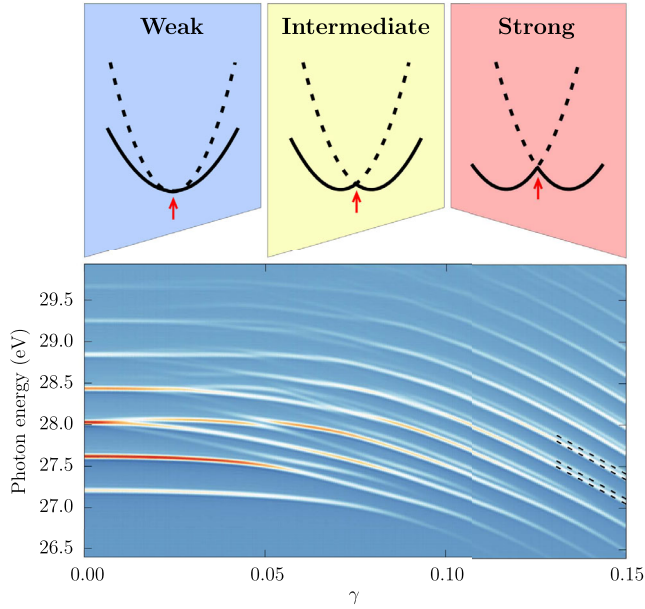


FIG. 2. (Bottom) XUV-only absorption spectrum as a function of γ [See Eq. (3)]. (Top) The adiabatic potential energy curves as a function of Q_2 for $\dot{Q}_2 = 0$ and for $\gamma = 0.00$, $\gamma = 0.05$, and $\gamma = 0.15$, respectively. We use $Q_1 = \dot{Q}_1 = 5.217$, which makes the figure independent of κ . Full and dashed lines show the adiabatic PESs of $|\phi_2^{(a)}\rangle$ and $|\phi_3^{(a)}\rangle$, respectively. The arrows are at $Q_2 = 0$ and indicate the position of the minimum of the PES for $|\phi_1^{(a)}\rangle$. The labels characterize the strength of the VC with respect to ATAS. The four dashed lines in the lower right of the bottom figure show selected adiabatic energies of the strongly VC-modified adiabatic potential.

We focus on the impact of the interstate coupling γ . The intrastate coupling κ also affects the dynamics. If we, e.g., consider the Landau-Zener model, the gradient of the diabatic PESs at the crossing, influenced by κ , plays an important role. The full exploration of the sensitivity to κ is left for future studies. Before we investigate the τ -dependent absorption, we present in Fig. 2 the XUV-only spectrum as a function of γ . The results allow us to divide the strength of the VC into three categories: weak, intermediate, and strong coupling. The weak coupling regime is characterized by spectra with weak dependence on γ , and due to the small off-diagonal components of ΔV , the wave function is approximately separable and the BOA well justified in the diabatic representation. Thus, the wave packet evolves almost exclusively on the surface of $|\phi_2^{(d)}\rangle$, and the spectrum is the one of the harmonic potential of the diabatic state with frequency $\omega = 0.015$. Delay-dependent absorption spectra calculated under the BOA are reported elsewhere [16]. In brief, in this weak coupling regime, ATAS spectra show clear signatures of the vibrational states, and a Fourier transform of the spectra with respect to τ confirms a modulation with the vibrational frequencies in question [18]. In the rest of this Letter, we therefore focus on the intermediate and strong coupling regimes.

As the VC strength is increased, the nonadiabatic electron-nuclear coupling can no longer be neglected and the BOA breaks down. As seen in the lower panel of Fig. 2, for increasing γ , we first go through an intermediate region characterized by more complex structures, such as avoided crossings of the absorption lines. These complex structures result from the simultaneous evolution of the wave packet on the coupled surfaces of $|\phi_2^{(d)}\rangle$ and $|\phi_3^{(d)}\rangle$, leading to a strong anharmonicity in the spectra. When γ is increased further, we reach the strong coupling region with a relatively simple and well-ordered spectrum. In the top panels of Fig. 2, we show a sketch of the PESs in the Q_2 direction. As γ is increased, a double-well structure emerges in the γ -distorted adiabatic PES for $|\phi_2^{(a)}\rangle$ (full curve). The VC is so strong that the entire wave packet follows this strongly modified adiabatic excited state surface. In the bottom right of Fig. 2, we see that the absorption lines follow the energies of the field-free vibrational states of the adiabatic PES corresponding to $|\phi_2^{(a)}\rangle$, which validates that the nuclear wave packet is confined to move on a single strongly modified adiabatic PES. The energy splitting between the doublets in this limit is ≈ 0.3 eV, which corresponds to a revival period of ≈ 13.5 fs; a period we will see later. For now, we stress that this period differs from the periods associated with the harmonic diabatic potentials of $|\phi_2^{(d)}\rangle$ and $|\phi_3^{(d)}\rangle$ (10 and 15 fs, respectively) and is hence a signature of anharmonic effects.

Equipped with the above knowledge of wave packet evolution under XUV-only conditions, we now turn to the study of τ -dependent spectra. In the XUV-only case, three electronic states were involved in the dynamics (Fig. 1), but now the electronic state $|\phi_4^{(d)}\rangle$ can be accessed through its NIR-induced dipole coupling with $|\phi_2^{(d)}\rangle$. The excited states can only be reached by the XUV, and not by the NIR. In Fig. 3, the delay-dependent absorption spectrum for $\gamma = 0.05$ is shown. This γ value places the VC strength in the intermediate region, where even the XUV-only spectra show rich structures (Fig. 2). For negative delays, the XUV pulse comes after the NIR pulse, and to the very left in Fig. 3, we therefore find a spectrum identical to the XUV-only spectrum. For larger delays, the NIR pulse strongly modifies the spectrum, and in opposition to other molecular ATAS spectra [16,18], the spectrum shows a complete lack of periodicity. The vibrational period $\omega_{2,1}$ in the Q_1 direction of the diabatic surface corresponding to the $|\phi_2^{(d)}\rangle$ state is 10 fs, but a Fourier analysis of the data in Fig. 3 shows no sign of any modulation at that or any other period, a signature of anharmonic effects. In addition, the ATAS spectrum in the intermediate VC regime is characterized by broad spectral features indicating shorter timescales, and therefore, as a consequence of the nonadiabatic coupling between electronic and nuclear degrees of freedom, nuclear

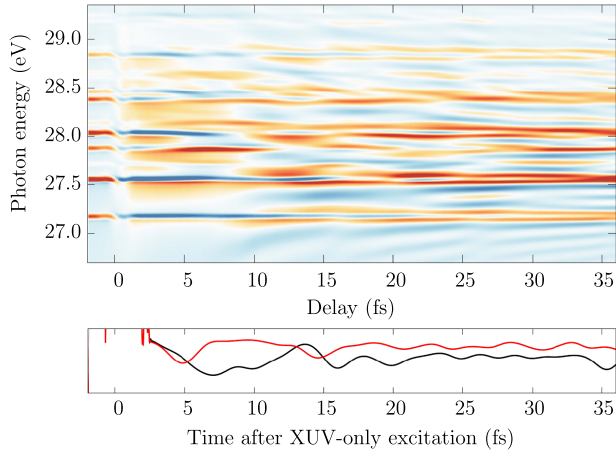


FIG. 3. ATAS spectrum for $\gamma = 0.05$ (intermediate region in Fig. 2) for different delays between the XUV and the NIR pulse. A positive delay denotes that the XUV comes before the NIR. The lower part of the figure is concerned with the XUV-only case. The XUV is fired at time zero and the time-dependent populations of the diabatic state $|\phi_2^{(d)}\rangle$ (black line) and the adiabatic state $|\phi_2^{(a)}\rangle$ (red line) are shown on an axis from 5.0×10^{-7} to 1.3×10^{-6} .

motion faster than the typical vibrational periods of the system. To further elucidate the dynamics in this regime, we show in the lower panel of Fig. 3 the time-dependent population of $|\phi_2^{(a)}\rangle$ and $|\phi_2^{(d)}\rangle$, found in an XUV-only calculation. In these populations, we observe no regular patterns and populations of similar magnitude, which is a signature of a relatively strong VC located in a spatial domain accessible for the nuclear wave packets. As a result, the nuclear dynamics is relatively fast and complex in both representations, due to the simultaneous motion of the wave packet on the two coupled electronic states. Even when the diabatic states are assumed to be harmonic, Eq. (1), the VC strongly affects the dynamics, and for nonvanishing γ , the harmonic frequencies of the PES are not observed in the ATAS or the XUV-only spectrum of Fig. 2.

In Fig. 4, the interstate coupling is increased to the strong VC domain, $\gamma = 0.15$ (Fig. 2). The ATAS spectrum in Fig. 4 is very different from the one in Fig. 3. *A priori*, the dominant periodic modulations seen in the spectrum of Fig. 4 bear strong similarities with spectra in the weak VC domain. The nuclear wave packets, however, now move on strongly modified PESs mixing the Q_1 and Q_2 directions (Fig. 5). Remember the XUV-only case where the nuclear dynamics in the adiabatic representation was particularly simple in the strong coupling regime with only the PES corresponding to $|\phi_2^{(a)}\rangle$ populated. The dynamics in this regime is illustrated in Fig. 5, which shows the evolution of the density of the full wave packet in the excited states and the period of the XUV-induced wave packet motion is exactly the 13.5 fs also seen in the lower panel of Fig. 4, and corresponding to the revival period for the wave packet in the adiabatic surface [see dashed lines in the lower panel

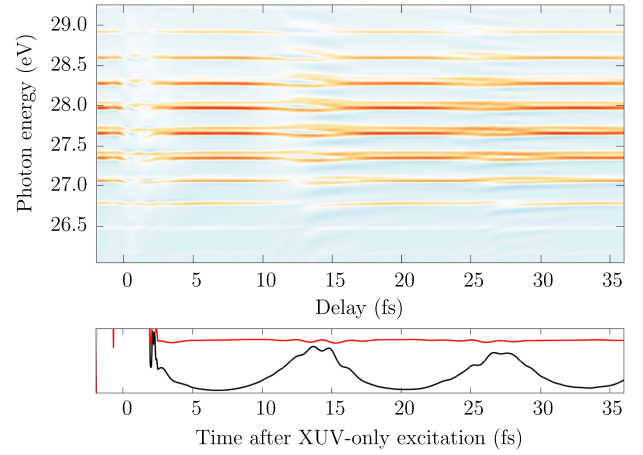


FIG. 4. As Fig. 3 but for $\gamma = 0.15$ (strong region in Fig. 2) and with a scale for the time-dependent populations in the lower part from 3.0×10^{-7} to 1.4×10^{-6} .

of Fig. 2]. With the NIR field present, the $|\phi_2^{(d)}\rangle$ state is coupled to the $|\phi_4^{(d)}\rangle$ state. We therefore expect the time-dependent dipole moment, and thereby the absorption signal, to be weaker for delays where population can be trapped in the $|\phi_4^{(d)}\rangle$ state, i.e., at delays where the nuclear wave packet is located in $|\phi_2^{(d)}\rangle$. The lower panel of Fig. 4 validates this hypothesis: the peaks in the diabatic population aligns with the absorption dips observed in the

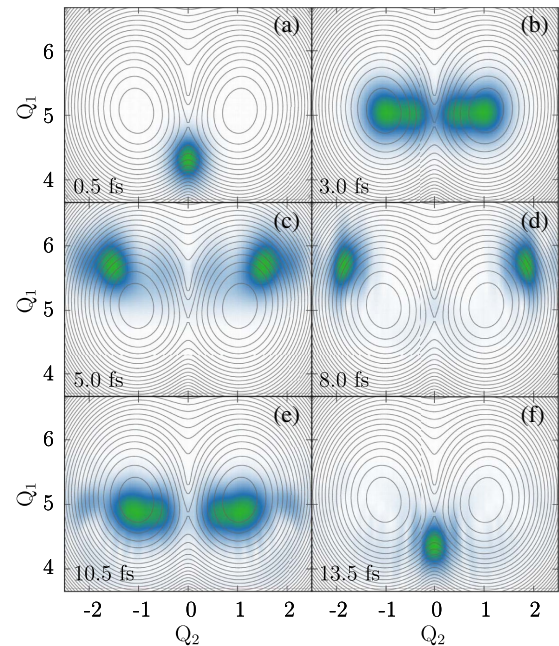


FIG. 5. Evolution of the density of the nuclear wave packet in the excited states at the instants indicated in (a)–(f) for $\gamma = 0.15$ and the XUV-only case as in the lower panel of Fig. 4. The contours represent the adiabatic PES for the $|\phi_2^{(a)}\rangle$ state. The figure shows the oscillation period observed in Fig. 4.

upper panel. We also see from the lower panel of Fig. 4 that the adiabatic population is almost constant, which is again a signature of the strong VC domain. In [25], the case of unequal frequencies along the different vibrational modes is considered. Also in that case, a revival-like behavior can be observed in the excited state density, and the conclusions from the strong coupling regime therefore hold for this case as well.

In summary, based on a minimal extension of a vibronic coupling model, which has been successfully used for more than 40 years [23,24], we investigated attosecond-resolved absorption spectra for a molecule in the vicinity of a CI accessible by attosecond pulse excitation from the ground state. We showed examples of how the CI induces different dynamics depending on the VC strength and illustrated the signatures of these dynamics in the spectra. We divided the VC strength into weak, intermediate, and strong coupling domains. Detailed information about the resulting nuclear and electronic dynamics can be obtained from time-resolved ATAS measurements. The results of this Letter can be used for generic identification and characterization of CIs in experimental ATAS data, emphasizing the general aspects of the problem in this theory work and leaving consideration of particular molecules for future studies.

This work was supported by the Villum Kann Rasmussen (VKR) Center of Excellence QUSCOPE.

-
- [1] D. R. Yarkony, Diaboliical conical intersections, *Rev. Mod. Phys.* **68**, 985 (1996).
- [2] W. Domcke and D. R. Yarkony, Role of conical intersections in molecular spectroscopy and photoinduced chemical dynamics, *Annu. Rev. Phys. Chem.* **63**, 325 (2012).
- [3] *Conical Intersections: Electronic Structure, Dynamics and Spectroscopy*, edited by W. Domcke, D. R. Yarkony, and H. Köppel, Advanced Series in Physical Chemistry Vol. 15 (World Scientific, Singapore, 2004).
- [4] D. Polli, P. Altoè, O. Weingart, K. M. Spillane, C. Manzoni, D. Brida, G. Tomasello, G. Orlandi, P. Kukura, R. A. Mathies, M. Garavelli, and G. Cerullo, Conical intersection dynamics of the primary photoisomerization event in vision, *Nature (London)* **467**, 440 (2010).
- [5] H. Timmers, Z. Li, N. Shivaram, R. Santra, O. Vendrell, and A. Sandhu, Coherent Electron Hole Dynamics near a Conical Intersection, *Phys. Rev. Lett.* **113**, 113003 (2014).
- [6] T. A. A. Oliver, N. H. C. Lewis, and G. R. Fleming, Correlating the motion of electrons and nuclei with two-dimensional electronic-vibrational spectroscopy, *Proc. Natl. Acad. Sci. U.S.A.* **111**, 10061 (2014).
- [7] M. Kowalewski, K. Bennett, J. R. Rouxel, and S. Mukamel, Monitoring Nonadiabatic Electron-Nuclear Dynamics in Molecules by Attosecond Streaking of Photoelectrons, *Phys. Rev. Lett.* **117**, 043201 (2016).
- [8] M. Kowalewski, K. Bennett, K. E. Dorfman, and S. Mukamel, Catching Conical Intersections in the Act: Monitoring Transient Electronic Coherences by Attosecond Stimulated X-Ray Raman Signals, *Phys. Rev. Lett.* **115**, 193003 (2015).
- [9] C. Arnold, O. Vendrell, R. Welsch, and R. Santra, Control of Nuclear Dynamics through Conical Intersections and Electronic Coherences, *Phys. Rev. Lett.* **120**, 123001 (2018).
- [10] M. Wu, S. Chen, S. Camp, K. J. Schafer, and M. B. Gaarde, Theory of strong-field attosecond transient absorption, *J. Phys. B* **49**, 062003 (2016).
- [11] E. Goulielmakis, Z.-H. Loh, A. Wirth, R. Santra, N. Rohringer, V. S. Yakovlev, S. Zherebtsov, T. Pfeifer, A. M. Azzeer, M. F. Kling, S. R. Leone, and F. Krausz, Real-time observation of valence electron motion, *Nature (London)* **466**, 739 (2010).
- [12] H. Wang, M. Chini, S. Chen, C.-H. Zhang, F. He, Y. Cheng, Y. Wu, U. Thumm, and Z. Chang, Attosecond Time-Resolved Autoionization of Argon, *Phys. Rev. Lett.* **105**, 143002 (2010).
- [13] M. Holler, F. Schapper, L. Gallmann, and U. Keller, Attosecond Electron Wave-Packet Interference Observed by Transient Absorption, *Phys. Rev. Lett.* **106**, 123601 (2011).
- [14] S. Chen, M. J. Bell, A. R. Beck, H. Mashiko, M. Wu, A. N. Pfeiffer, M. B. Gaarde, D. M. Neumark, S. R. Leone, and K. J. Schafer, Light-induced states in attosecond transient absorption spectra of laser-dressed helium, *Phys. Rev. A* **86**, 063408 (2012).
- [15] C. Ott, A. Kaldun, P. Raith, K. Meyer, M. Laux, J. Evers, C. H. Keitel, C. H. Greene, and T. Pfeifer, Lorentz meets Fano in spectral line shapes: a universal phase and its laser control, *Science* **340**, 716 (2013).
- [16] J. E. Bækhoj, L. Yue, and L. B. Madsen, Nuclear-motion effects in attosecond transient-absorption spectroscopy of molecules, *Phys. Rev. A* **91**, 043408 (2015).
- [17] J. E. Bækhoj and L. B. Madsen, Light-induced structures in attosecond transient-absorption spectroscopy of molecules, *Phys. Rev. A* **92**, 023407 (2015).
- [18] E. R. Warrick, J. E. Bækhoj, W. Cao, A. P. Fidler, F. Jensen, L. B. Madsen, S. R. Leone, and D. M. Neumark, Attosecond transient absorption spectroscopy of molecular nitrogen: Vibrational coherences in the $b' \ ^1\Sigma_u^+$ state, *Chem. Phys. Lett.* **683**, 408 (2017).
- [19] M. Hollstein, R. Santra, and D. Pfannkuche, Correlation-driven charge migration following double ionization and attosecond transient absorption spectroscopy, *Phys. Rev. A* **95**, 053411 (2017).
- [20] Y. Cheng, M. Chini, X. Wang, A. González-Castrillo, A. Palacios, L. Argenti, F. Martín, and Z. Chang, Reconstruction of an excited-state molecular wave packet with attosecond transient absorption spectroscopy, *Phys. Rev. A* **94**, 023403 (2016).
- [21] L. J. Borja, M. Zürich, C. D. Pemmaraju, M. Schultze, K. Ramasesha, A. Gandman, J. S. Prell, D. Prendergast, D. M. Neumark, and S. R. Leone, Extreme ultraviolet transient absorption of solids from femtosecond to attosecond time-scales, *J. Opt. Soc. Am. B* **33**, C57 (2016).
- [22] A. Moulet, J. B. Bertrand, T. Klostermann, A. Guggenmos, N. Karpowicz, and E. Goulielmakis, Soft x-ray excitonics, *Science* **357**, 1134 (2017).
- [23] L. S. Cederbaum, W. Domcke, H. Köppel, and W. Von Niessen, Strong vibronic coupling effects in ionization

- spectra: The “mystery band” of butatriene, *Chem. Phys.* **26**, 169 (1977).
- [24] H. Köppel, W. Domcke, and L. S. Cederbaum, Multimode molecular dynamics beyond the Born-Oppenheimer approximation, *Adv. Chem. Phys.* **57**, 59 (1984).
- [25] See Supplemental Material at <http://link.aps.org/supplemental/10.1103/PhysRevLett.121.023203>, where the model parameters are given, details of the computational approach are discussed, and an example elucidates the sensitivity of the results to different frequencies of the harmonic potential energy surfaces along the two nuclear coordinates, which includes Refs. [26,27].
- [26] H. Köppel, L. S. Cederbaum, and W. Domcke, Strong nonadiabatic effects and conical intersections in molecular spectroscopy and unimolecular decay: $C_2H_4^+$, *J. Chem. Phys.* **77**, 2014 (1982).
- [27] C. Cattarius, G. A. Worth, H.-D. Meyer, and L. S. Cederbaum, All mode dynamics at the conical intersection of an octatomic molecule: Multi-configuration time-dependent Hartree (MCTDH) investigation on the butatriene cation, *J. Chem. Phys.* **115**, 2088 (2001).
- [28] M. B. Gaarde, C. Buth, J. L. Tate, and K. J. Schafer, Transient absorption and reshaping of ultrafast XUV light by laser-dressed helium, *Phys. Rev. A* **83**, 013419 (2011).
- [29] In Ref. [16], the relation of $S(\omega, \tau)$ to other measures of absorption is discussed.
- [30] M. D. Feit, J. A. Fleck, Jr., and A. Steiger, Solution of the Schrödinger equation by a spectral method, *J. Comput. Phys.* **47**, 412 (1982).